

Strain-modulated anisotropic Andreev reflection in a graphene-based superconducting junction

Xingfei Zhou(周兴飞), Ziming Xu (许子铭), Deliang Cao(曹德亮), and Fenghua Qi(戚凤华)
Citation: Chin. Phys. B, 2022, 31 (**11**): 117403. DOI: 10.1088/1674-1056/ac7553

What follows is a list of articles you may be interested in

Electronic properties and interfacial coupling in Pb islands on single-crystalline graphene

Jing-Peng Song(宋靖鹏) and Ang Li(李昂)
Chin. Phys. B, 2022, 31 (**3**): 037401. DOI: 10.1088/1674-1056/ac1b8e

Superconductivity in octagraphene

Jun Li(李军) and Dao-Xin Yao(姚道新)
Chin. Phys. B, 2022, 31 (**1**): 017403. DOI: 10.1088/1674-1056/ac40fa

Temperature and doping dependent flat-band superconductivity on the Lieb-lattice

Feng Xu(徐峰), Lei Zhang(张磊), and Li-Yun Jiang(姜立运)
Chin. Phys. B, 2021, 30 (**6**): 067401. DOI: 10.1088/1674-1056/abdea5

Effect of graphene grain boundaries on MoS_2/graphene heterostructures

Yue Zhang(张悦), Xiangzhe Zhang(张祥喆), Chuyun Deng(邓楚芸), Qi Ge(葛奇), Junjie Huang(黄俊杰), Jie Lu(卢捷), Gaoxiang Lin(林高翔), Zekai Weng(翁泽锴), Xueao Zhang(张学骜), Weiwei Cai(蔡伟伟)
Chin. Phys. B, 2020, 29 (**6**): 067403. DOI: 10.1088/1674-1056/ab8a37

Application of graphene vertical field effect to regulation of organic light-emitting transistors

Hang Song(宋航), Hao Wu(吴昊), Hai-Yang Lu(陆海阳), Zhi-Hao Yang(杨志浩), Long Ba(巴龙)
Chin. Phys. B, 2020, 29 (**5**): 057401. DOI: 10.1088/1674-1056/ab81f3

Strain-modulated anisotropic Andreev reflection in a graphene-based superconducting junction

Xingfei Zhou(周兴飞)[1,†], Ziming Xu (许子铭)[1], Deliang Cao(曹德亮)[1], and Fenghua Qi(戚凤华)[2,‡]

[1] *New Energy Technology Engineering Laboratory of Jiangsu Province, School of Science, Nanjing University of Posts and Telecommunications, Nanjing* 210023, *China*

[2] *School of Electronic Engineering, Nanjing Xiaozhuang University, Nanjing* 211171, *China*

(Received 26 January 2022; revised manuscript received 20 May 2022; accepted manuscript online 2 June 2022)

We investigate the Andreev reflection across a uniaxial strained graphene-based superconducting junction. Compared with pristine graphene-based superconducting junction, three opposite properties are found. Firstly, in the regime of the interband conversion of electron–hole, the Andreev retro-reflection happens. Secondly, in the regime of the intraband conversion of electron–hole, the specular Andreev reflection happens. Thirdly, the perfect Andreev reflection, electron–hole conversion with unit efficiency, happens at a nonzero incident angle of electron. These three exotic properties arise from the strain-induced anisotropic band structure of graphene, which breaks up the original relation between the direction of velocity of particle and the direction of the corresponding wavevector. Our finding gives an insight into the understanding of Andreev reflection and provides an alternative method to modulate the Andreev reflection.

Keywords: graphene, uniaxial strain, anisotropic Andreev reflection

PACS: 74.45.+c, 73.23.Ad, 85.25.–j **DOI:** 10.1088/1674-1056/ac7553

1. Introduction

Graphene, a single atomic plane of graphite with a two-dimensional honeycomb lattice,[1] provides a highly practical and prospective platform for studying basic physics and applied physics, such as half-integer quantum Hall effect,[2] Klein tunneling,[3] specular Andreev reflection,[4] topological phase transition,[5–8] superconductivity,[9–12] next-generation electronics and photonics,[13,14] and heterostructure.[15] In the first Brillouin zone, there are two inequivalent corners K and K', around which is a conical band structure described by the massless Dirac equation. When a uniaxial strain is applied in graphene, the tilted Dirac cone is found,[16,17] which leads to the same structure of relativistic Landau levels as in pristine graphene, but with a renormalized effective Fermi velocity. In this work, we will show that the uniaxial strain can induce anisotropic and interesting Andreev reflection.

In a normal metal–superconductor (s-wave pairing) junction, when an electron from normal region hits the interface of junction, a hole is reflected to the normal region and a pair of electron coupling a Cooper pair is injected into the s-wave pairing superconductor, known as Andreev reflection.[18] Owing to the same path of incident electron and reflected hole in the same band (intraband conversion of electron–hole), this process is also called Andreev retro-reflection (ARR). However, the specular Andreev reflection (SAR) was found in a graphene-based superconducting junction,[4] where electron and hole belong to different bands (interband conversion of electron–hole) and then the paths of electron and hole are specular. After that, Andreev reflection is widely studied in many Dirac materials and a general view of intraband (interband) conversion-induced ARR (SAR) is left gradually.[19–35] Whereas, an opposite view, i.e., interband (intraband) conversion-induced ARR (SAR), was shown in the two-dimensional electron gas system with Rashba spin–orbit coupling,[36] the 8-*Pmmn* borophene (borophane)-based superconducting junction,[37–39] and the tilted Weyl semimetal hybrid junction.[40] Although only the intraband (interband) conversion-induced ARR (SAR) is believed to happen in graphene previously, in this work, we will show that the interband (intraband) conversion-induced ARR (SAR) can also happen in graphene by applying a uniaxial strain. Besides, we will show that the perfect Andreev reflection, electron–hole conversion with unit efficiency, exists at a nonzero incident angle in graphene, which breaks the previous view that the perfect Andreev reflection only happens at normal incidence in graphene.

The paper is organized as follows. We firstly give the model and basic formalism. Then, the numerical results and theoretical analysis are presented and discussed. Finally, the main results of this work are summarized.

2. Models and methods

For the pristine graphene, the distance between nearest-neighbor (next-nearest-neighbor) carbon atoms is denoted by $a = 0.142$ nm ($b = \sqrt{3}a$). The nearest neighbor (next-nearest neighbor) hopping amplitude is denoted by $t = 3$ eV ($t_{\rm nnn} =$

†Corresponding author. E-mail: zxf@njupt.edu.cn

‡Corresponding author. E-mail: qifenghua@njxzc.edu.cn

© 2022 Chinese Physical Society and IOP Publishing Ltd

$0.1t$). When a uniaxial strain along y direction is considered, as shown in Fig. 1, the distance between nearest neighbor atoms along y axis changes from a to $a' = a(1+\zeta)$ in which $\zeta = \delta a/a$ is the lattice deformation measuring the strain amplitude. The model for strained graphene-based normal metal–superconductor (NS) junction is shown in Fig. 1. The electron and hole excitations are described by the Dirac–Bogoliubov–de Gennes (DBdG) equation[4]

$$\begin{pmatrix} \mathcal{H}_\eta - E_{\rm F} & \Delta_0 \mathrm{e}^{\mathrm{i}\phi} \\ \Delta_0 \mathrm{e}^{-\mathrm{i}\phi} & E_{\rm F} - \mathcal{H}_\eta \end{pmatrix} \begin{pmatrix} u_{\rm e} \\ v_{\rm h} \end{pmatrix} = \varepsilon \begin{pmatrix} u_{\rm e} \\ v_{\rm h} \end{pmatrix}. \tag{1}$$

Here $\mathcal{H}_\eta = \eta(\hbar v_x \sigma_x k_x + \hbar v_y \sigma_y k_y + \hbar v_{\rm t} \sigma_0 k_x) - U\sigma_0$ in which the anisotropic velocities are $v_x = \sqrt{3}at\sin\alpha$ and $v_y = \frac{3}{2}at'(1+\frac{2}{3}\zeta)$, the tilted velocity is $v_{\rm t} = 2\sqrt{3}(at_{\rm nnn}\sin 2\alpha + at'_{\rm nnn}\sin\alpha)$ with $t_{\rm nnn} = 0.1t$, $t'_{\rm nnn} = t_{\rm nnn}(1-2\zeta+\frac{b}{2d}\zeta)$, $t' = t(1-2\zeta)$, and $\alpha = \arccos(-t'/2t)$. t' ($t'_{\rm nnn}$) is the hopping amplitude between nearest neighbor (next-nearest neighbor) carbon atoms separated by the deformed lattice distance a'. $d \approx a/3.5$ is a characteristic distance related to the overlap of atomic orbitals. $\eta = +(-)$ denote D (D′) valley index, which is shifted away from the high-symmetry points K (K').[16] In DBdG equation, η has another meaning, i.e., $\eta = 1\,(-1)$ represents the incident electron from D (D′) valley and the reflected hole back to D′ (D) valley. $\sigma_{x,y}$ and σ_0 represent the 2×2 Pauli matrix and unit matrix, respectively. $U = U_0\Theta(x')$ with the Heaviside step function Θ can be adjusted by doping or a gate voltage in the superconducting region and is zero in the normal region. Fermi energy of system is denoted by $E_{\rm F}$. The macroscopic phase in the superconducting region is denoted by ϕ. ε is the excited energy (relative to the Fermi energy) of electron and hole. $u_{\rm e}$ and $v_{\rm h}$ represent the electron and hole wavefunctions in the normal region, respectively. In the superconducting region, $u_{\rm e}$ and $v_{\rm h}$ denote the electron-like and hole-like wavefunctions, respectively. The zero temperature energy-gap function in the superconducting region is represented by Δ_0.

From Eq. (2), the excited spectrum of electron and hole in the normal region are calculated as

$$\begin{aligned} \varepsilon_{\rm e}^{\pm} &= \eta\hbar v_{\rm t} k_x^{\rm e} \pm \hbar\sqrt{(v_x k_x^{\rm e})^2 + (v_y k_y^{\rm e})^2} - E_{\rm F}, \\ \varepsilon_{\rm h}^{\pm} &= -\eta\hbar v_{\rm t} k_x^{\rm h} \pm \hbar\sqrt{(v_x k_x^{\rm h})^2 + (v_y k_y^{\rm h})^2} + E_{\rm F}. \end{aligned} \tag{2}$$

Here $+(-)$ denotes the electron in the conduction (valence) band and the hole in the valence (conduction). Similarly, the excited spectrum of electron-like and hole-like particles in superconducting region are obtained

$$\begin{aligned} &\eta\hbar v_{\rm t} k_x^{\rm se} + \hbar\sqrt{(v_x k_x^{\rm se})^2 + (v_y k_y^{\rm se})^2} \\ &= E_{\rm F} + U_0 + \sqrt{\varepsilon^2 + \Delta^2}, \\ &\eta\hbar v_{\rm t} k_x^{\rm sh} + \hbar\sqrt{(v_x k_x^{\rm sh})^2 + (v_y k_y^{\rm sh})^2} \\ &= E_{\rm F} + U_0 - \sqrt{\varepsilon^2 + \Delta^2}. \end{aligned} \tag{3}$$

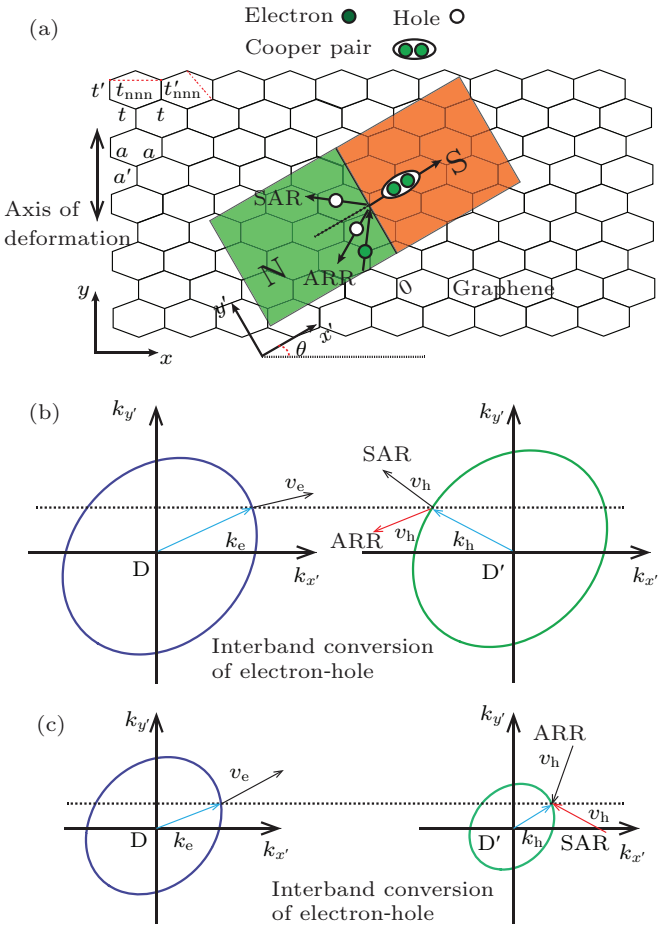


Fig. 1. (a) Schematic diagrams for strained graphene-based superconducting junction. The direction of junction is characterized by θ. The bonds parallel to the deformation axis are modified. The pristine (deformed) lattice distance is denoted by a (a'). t ($t_{\rm nnn}$) represents the nearest neighbor (next-nearest neighbor) hopping amplitude without deformation. t' ($t'_{\rm nnn}$) is the hopping amplitude between nearest neighbor (next-nearest neighbor) carbon atoms separated by the deformed lattice distance a'. Schematic diagrams for SAR and ARR through the equal energy surfaces of electron and hole with (b) $E_{\rm F} = 0$ or (c) $E_{\rm F} = \Delta_0 = 10$ meV and $\theta = \pi/4$. The black dotted line denotes the conservation of transverse wave vector $k_{y'}$ in the process of transmission. The incident electron comes from D valley and the reflected hole returns to D′ valley. The direction of wavevector is different from the direction of velocity due to the anisotropic band structure of strained graphene, which makes interband-induced ARR and intraband-induced SAR possible.

According to Fig. 1(a), the relation of the wavevector components in coordinate systems x–y and x'–y' meets[30,41]

$$\begin{cases} k_x = k_{x'}\cos\theta - k_{y'}\sin\theta, \\ k_y = k_{x'}\sin\theta + k_{y'}\cos\theta. \end{cases} \tag{4}$$

Here the direction of x'-axis is perpendicular to the interface of superconducting junction, as shown in Fig. 1(a). θ is the angle between x-axis and x'-axis. By substituting Eq. (4) into Eq. (2), the excited spectrum of electron and hole in the normal region in coordinate system x'–y' can be obtained. The schematic diagrams for SAR and ARR through the equal energy surfaces of electron and hole with $E_{\rm F} = 0$ ($E_{\rm F} = \Delta_0$) and

$\theta = \pi/4$ are drawn in Fig. 1(b) (Fig. 1(c)). Generally, the direction of velocity parallels the direction of wavevector when the band structure is isotropic. But, the direction of wavevector is different from the direction of velocity due to the anisotropic band structure of strained graphene, which makes interband-induced ARR and intraband-induced SAR possible.

In the coordinate system x'–y', owing to the continuity of wavefunctions, the wavefunctions at the interface of NS junction meet

$$\psi^{\eta}_{\mathrm{e}+} + r\psi^{\eta}_{\mathrm{e}-} + r_{\mathrm{a}}\psi^{\eta}_{\mathrm{h}-} = a\psi^{\eta}_{\mathrm{se}} + b\psi^{\eta}_{\mathrm{sh}}, \tag{5}$$

where $\psi^{\eta}_{\mathrm{e}+}$ ($\psi^{\eta}_{\mathrm{e}-}$) denotes the wavefunction of incident (reflected) electron towards (away) the interface in the normal region, $\psi^{\eta}_{\mathrm{h}-}$ represents the wavefunction of reflected hole away the interface in the normal region, and $\psi^{\eta}_{\mathrm{se}}$ ($\psi^{\eta}_{\mathrm{sh}}$) denotes the electron-like (hole-like) wavefunction in the superconducting region. In the coordinate system x'–y', the corresponding component of momentum $k_{y'}$ is conserved due to the translational invariance in y' direction. Then, when the excited energy ε and transverse momentum $k_{y'}$ are given, the detailed forms of wavefunctions above are calculated as

$$\begin{aligned}
\psi^{\eta}_{\mathrm{e}+} &= \mathrm{e}^{\mathrm{i}k^{\mathrm{i}}_{x'\mathrm{e}}x' + \mathrm{i}k_{y'}y'}(1, \kappa_{\mathrm{ei}}, 0, 0)^{\mathrm{T}},\\
\psi^{\eta}_{\mathrm{e}-} &= \mathrm{e}^{\mathrm{i}k^{\mathrm{r}}_{x'\mathrm{e}}x' + \mathrm{i}k_{y'}y'}(1, \kappa_{\mathrm{er}}, 0, 0)^{\mathrm{T}},\\
\psi^{\eta}_{\mathrm{h}-} &= \mathrm{e}^{\mathrm{i}k^{\mathrm{r}}_{x'\mathrm{h}}x' + \mathrm{i}k_{y'}y'}(0, 0, 1, \kappa_{\mathrm{hr}})^{\mathrm{T}},\\
\psi^{\eta}_{\mathrm{se}} &= \mathrm{e}^{\mathrm{i}k^{\mathrm{se}}_{x'}x' + \mathrm{i}k_{y'}y'}(\mathrm{e}^{\mathrm{i}\beta}, \kappa_{\mathrm{se}}\mathrm{e}^{\mathrm{i}\beta}, \mathrm{e}^{-\mathrm{i}\phi}, \kappa_{\mathrm{se}}\mathrm{e}^{-\mathrm{i}\phi})^{\mathrm{T}},\\
\psi^{\eta}_{\mathrm{sh}} &= \mathrm{e}^{\mathrm{i}k^{\mathrm{sh}}_{x'}x' + \mathrm{i}k_{y'}y'}(\mathrm{e}^{-\mathrm{i}\beta}, \kappa_{\mathrm{sh}}\mathrm{e}^{-\mathrm{i}\beta}, \mathrm{e}^{-\mathrm{i}\phi}, \kappa_{\mathrm{sh}}\mathrm{e}^{-\mathrm{i}\phi})^{\mathrm{T}},
\end{aligned} \tag{6}$$

where

$$\begin{aligned}
\kappa_{\mathrm{ei(r)}} &= \eta\frac{\hbar v_x k^{\mathrm{i(r)}}_{x\mathrm{e}} + \mathrm{i}\hbar v_y k^{\mathrm{i(r)}}_{y\mathrm{e}}}{\varepsilon - \eta\hbar v_{\mathrm{t}} k^{\mathrm{i(r)}}_{x\mathrm{e}} + E_{\mathrm{F}}},\\
\kappa_{\mathrm{hr}} &= -\eta\frac{\hbar v_x k^{\mathrm{r}}_{x\mathrm{h}} + \mathrm{i}\hbar v_y k^{\mathrm{r}}_{y\mathrm{h}}}{\varepsilon + \eta\hbar v_{\mathrm{t}} k^{\mathrm{r}}_{x\mathrm{h}} - E_{\mathrm{F}}},\\
\kappa_{\mathrm{se(sh)}} &= \eta\frac{v_x k^{\mathrm{se(sh)}}_{x} + \mathrm{i}v_y k^{\mathrm{se(sh)}}_{y}}{\sqrt{(v_x k^{\mathrm{se(sh)}}_{x})^2 + (v_y k^{\mathrm{se(sh)}}_{y})^2}},\\
\beta &= \begin{cases} \arccos(\varepsilon/\Delta_0) & \varepsilon < \Delta_0,\\ -\mathrm{i}\,\mathrm{arcosh}(\varepsilon/\Delta_0) & \varepsilon > \Delta_0. \end{cases}
\end{aligned} \tag{7}$$

Here the values of all wavevectors can be obtained by Eqs. (2)–(4). By substituting Eq. (6) into Eq. (5), the reflected coefficient r and Andreev reflected coefficient r_{a} are derived as

$$\begin{aligned}
r &= \frac{(\kappa_{\mathrm{hr}} - \kappa_{\mathrm{se}})(\kappa_{\mathrm{ei}} - \kappa_{\mathrm{sh}}) + (\kappa_{\mathrm{se}} - \kappa_{\mathrm{ei}})(\kappa_{\mathrm{hr}} - \kappa_{\mathrm{sh}})}{(\kappa_{\mathrm{hr}} - \kappa_{\mathrm{se}})(\kappa_{\mathrm{sh}} - \kappa_{\mathrm{er}}) + (\kappa_{\mathrm{er}} - \kappa_{\mathrm{se}})(\kappa_{\mathrm{hr}} - \kappa_{\mathrm{sh}})},\\
r_{\mathrm{a}} &= \frac{(\kappa_{\mathrm{ei}} - \kappa_{\mathrm{er}})(\kappa_{\mathrm{se}} - \kappa_{\mathrm{sh}})\,\mathrm{e}^{\mathrm{i}(\beta-\phi)}}{(\kappa_{\mathrm{hr}} - \kappa_{\mathrm{se}})(\kappa_{\mathrm{er}} - \kappa_{\mathrm{sh}}) - (\kappa_{\mathrm{er}} - \kappa_{\mathrm{se}})(\kappa_{\mathrm{hr}} - \kappa_{\mathrm{sh}})}.
\end{aligned} \tag{8}$$

In our paper, the Hamiltonian of strained graphene is rewritten as $H_\eta = \eta(\hbar S_x k_{x'} + \hbar S_y k_{y'})$ with $S_x = v_x\sigma_x\cos\theta + v_y\sigma_y\sin\theta + v_{\mathrm{t}}\sigma_0\cos\theta$ and $S_y = -v_x\sigma_x\sin\theta + v_y\sigma_y\cos\theta - v_{\mathrm{t}}\sigma_0\sin\theta$ in the coordinate system x'–y'. The probability current is conserved in x' direction, then, by using the same derivation in Ref. [41], the corresponding incident (reflected) probability current of electron along x' direction is calculated as $J_{x'\mathrm{ei}} = \eta\psi^{\eta\dagger}_{\mathrm{ei}}S_x\psi^{\eta}_{\mathrm{ei}}$ ($J_{x'\mathrm{er}} = \eta r^* r\psi^{\eta\dagger}_{\mathrm{er}}S_x\psi^{\eta}_{\mathrm{er}}$) and the corresponding reflected probability current of hole is calculated as $J_{x'\mathrm{hr}} = \eta r^*_{\mathrm{a}} r_{\mathrm{a}}\psi^{\eta\dagger}_{\mathrm{hr}}S_x\psi^{\eta}_{\mathrm{hr}}$. So the reflected and Andreev reflected probabilities are written as $R^{\eta} = |J_{x'\mathrm{er}}/J_{x'\mathrm{ei}}|$ and $R^{\eta}_{\mathrm{a}} = |J_{x'\mathrm{hr}}/J_{x'\mathrm{ei}}|$, respectively.

3. Results and discussion

3.1. Anisotropic Andreev reflection

In the coordinate x'–y', the velocity of incident electron along the x' (y') direction is obtained by $u^{\eta}_{x'(y')\mathrm{e}} = \frac{\partial\varepsilon^{\pm}_{\mathrm{e}}}{\hbar\partial k^{\mathrm{e}}_{x'(y')}}$ and the velocity of reflected hole along the x' (y') direction is obtained by $u^{\eta}_{x'(y')\mathrm{h}} = \frac{\partial\varepsilon^{\pm}_{\mathrm{h}}}{\hbar\partial k^{\mathrm{h}}_{x'(y')}}$. The signs of $u^{\eta}_{x'\mathrm{e}}$ and $u^{\eta}_{x'\mathrm{h}}$ are opposite all the time. When the signs of $u^{\eta}_{y'\mathrm{e}}$ and $u^{\eta}_{y'\mathrm{h}}$ are the same (opposite), the SAR (ARR) happens. From the view of incident and reflected angles, the incident angle of electron $\varphi^{\eta}_{\mathrm{ei}} = \arctan(u^{\eta}_{y'\mathrm{e}}/u^{\eta}_{x'\mathrm{e}})$ and the reflected angle of hole $\varphi^{\eta}_{\mathrm{hr}} = \arctan(u^{\eta}_{y'\mathrm{h}}/u^{\eta}_{x'\mathrm{h}})$ have the opposite (same) signs for SAR (ARR). In the follow process of calculation, we set $\zeta = 10\%$. In experiment, lattice deformation in graphene is estimated to the approximated value 12%.[42,43]

In the regime of electron–hole conversion in the interband ($E_{\mathrm{F}} = 0$), as shown in Fig. 2, the incident electron comes from the conduction band and $\varphi^{\eta}_{\mathrm{ei}}$-dependent $\varphi^{\eta}_{\mathrm{hr}}$ are plotted in $\theta = 0, \pi/4, \pi/3$, and $\pi/2$. When the signs of $\varphi^{\eta}_{\mathrm{ei}}$ and $\varphi^{\eta}_{\mathrm{hr}}$ are the same (opposite), ARR (SAR) happens, which are labeled in Fig. 2. In Fig. 2(a), by some simple calculations, we can obtain

$$\begin{aligned}
u^{\eta}_{y'\mathrm{e}} &= v_y^2 k_{y'}/\sqrt{(k^{\mathrm{e}}_{x'}v_x)^2 + (k_{y'}v_y)^2},\\
u^{\eta}_{y'\mathrm{h}} &= v_y^2 k_{y'}/\sqrt{(k^{\mathrm{h}}_{x'}v_x)^2 + (k_{y'}v_y)^2}.
\end{aligned}$$

Obviously, the signs of $u^{\eta}_{y'\mathrm{e}}$ and $u^{\eta}_{y'\mathrm{h}}$ are the same. Then, the signs of $\varphi^{\eta}_{\mathrm{ei}}$ and $\varphi^{\eta}_{\mathrm{hr}}$ are opposite due to the opposite signs of $u^{\eta}_{x'\mathrm{e}}$ and $u^{\eta}_{x'\mathrm{h}}$. Therefore, SAR happens, which is similar to the one in a pristine graphene-based superconducting junction.[4] However, in Figs. 2(b) and 2(c), we can obtain

$$\begin{aligned}
u^{\eta}_{y'\mathrm{e}} &= -\eta v_{\mathrm{t}}\sin\theta + \frac{-v_x^2 k^{\mathrm{e}}_x\sin\theta + v_y^2 k^{\mathrm{e}}_y\cos\theta}{\sqrt{(k^{\mathrm{e}}_x v_x)^2 + (k^{\mathrm{e}}_y v_y)^2}},\\
u^{\eta}_{y'\mathrm{h}} &= \eta v_{\mathrm{t}}\sin\theta + \frac{-v_x^2 k^{\mathrm{h}}_x\sin\theta + v_y^2 k^{\mathrm{h}}_y\cos\theta}{\sqrt{(k^{\mathrm{h}}_x v_x)^2 + (k^{\mathrm{h}}_y v_y)^2}}.
\end{aligned}$$

The presence of tilted velocity v_{t} and θ makes the opposite signs of $u^{\eta}_{y'\mathrm{e}}$ and $u^{\eta}_{y'\mathrm{h}}$ possible. In other words, the ARR may happen in the regime of electron–hole conversion in the interband. The numerical calculations in Figs. 2(b) and 2(c) show

that the ARR happens in an approximate range of φ_{ei}^{η} from -30° to 0°. In Fig. 2(d) with $\theta = \pi/2$, we can obtain

$$u_{y'e}^{\eta} = -\eta v_t + \frac{v_x^2 k_{y'}}{\sqrt{(k_{y'}v_x)^2 + (k_{x'}^{e}v_y)^2}},$$
$$u_{y'h}^{\eta} = \eta v_t + \frac{v_x^2 k_{y'}}{\sqrt{(k_{y'}v_x)^2 + (k_{x'}^{h}v_y)^2}}.$$

Obviously, the signs of $u_{y'e}^{\eta}$ and $u_{y'h}^{\eta}$ may be opposite due to the presence of tilted velocity v_t and then the ARR happens. The numerical calculations in Fig. 2(d) show that the ARR happens in an approximate range of φ_{ei}^{η} from -15° to 15°.

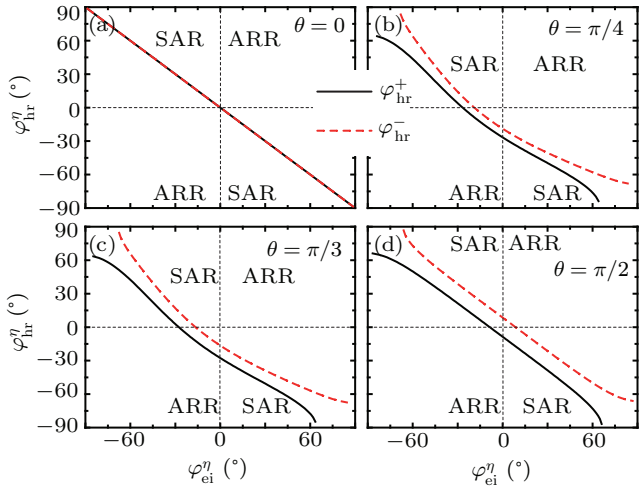


Fig. 2. (a)–(d) The incident angle of electron-dependent reflected angle of hole in the different directions of junction. The black (red dashed) line denotes the electron from D (D′) valley while the hole back to D′ (D) valley. Here $\Delta_0 = 10$ meV, $\varepsilon = 0.6\Delta_0$, and $E_F = 0$.

In the regime of electron–hole conversion in the intraband ($\varepsilon < E_F$), as shown in Fig. 3, the incident electron comes from the conduction band and φ_{ei}^{η}-dependent φ_{hr}^{η} are plotted in $\theta = 0$, $\pi/4$, $\pi/3$, and $\pi/2$. By calculations, we can obtain

$$u_{y'e}^{\eta} = -\eta v_t \sin\theta + \frac{-v_x^2 k_x^{e}\sin\theta + v_y^2 k_y^{e}\cos\theta}{\sqrt{(k_x^{e}v_x)^2 + (k_y^{e}v_y)^2}},$$
$$u_{y'h}^{\eta} = \eta v_t \sin\theta - \frac{-v_x^2 k_x^{h}\sin\theta + v_y^2 k_y^{h}\cos\theta}{\sqrt{(k_x^{h}v_x)^2 + (k_y^{h}v_y)^2}}.$$

Therefore, the signs of $u_{y'e}^{\eta}$ and $u_{y'h}^{\eta}$ are dependent on the direction of junction and the lattice deformation. In Fig. 3(a), it is easy to obtain

$$u_{y'e}^{\eta} = \frac{v_y^2 k_{y'}}{\sqrt{(k_{x'}^{e}v_x)^2 + (k_{y'}v_y)^2}},$$
$$u_{y'h}^{\eta} = -\frac{v_y^2 k_{y'}}{\sqrt{(k_{x'}^{h}v_x)^2 + (k_{y'}v_y)^2}},$$

which leads to the appearance of ARR due to the opposite signs of $u_{y'e}^{\eta}$ and $u_{y'h}^{\eta}$. This result is similar to the one in a pristine graphene-based superconducting junction.[4] Interestingly, an unusual phenomenon, i.e., intraband-induced SAR, is shown in Figs. 3(b)–3(c), which comes from the fact that the signs of $u_{y'e}^{\eta}$ and $u_{y'h}^{\eta}$ may be the same in the presence of tilted velocity v_t and θ. The numerical calculations in Figs. 3(b) and 3(c) show that the SAR happens in an approximate range of φ_{ei}^{η} from -15° to 0°. In Fig. 3(d) with $\theta = \pi/2$, we can obtain

$$u_{y'e}^{\eta} = -\eta v_t + \frac{v_x^2 k_{y'}}{\sqrt{(k_{y'}v_x)^2 + (k_{x'}^{e}v_y)^2}},$$
$$u_{y'h}^{\eta} = \eta v_t - \frac{v_x^2 k_{y'}}{\sqrt{(k_{y'}v_x)^2 + (k_{x'}^{h}v_y)^2}}.$$

When $v_t = 0$, it is easy to find that the signs of $u_{y'e}^{\eta}$ and $u_{y'h}^{\eta}$ are opposite, which means only the presence of ARR. However, the numerical calculations in Fig. 3(d) show that the SAR happens in an approximate range of φ_{ei}^{η} from -5° to 5° due to the presence of tilted velocity v_t.

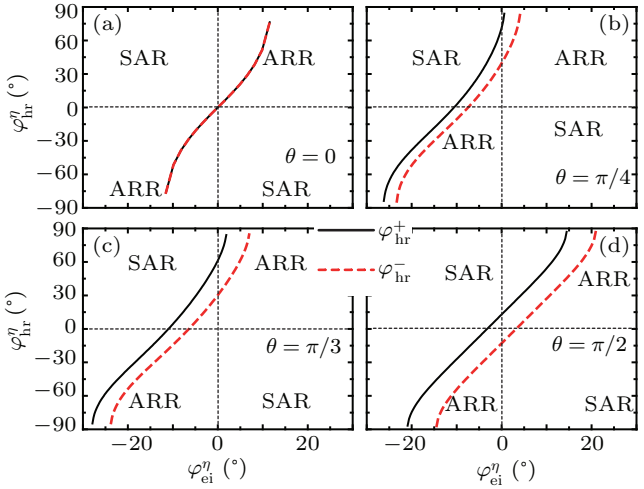


Fig. 3. (a)–(d) The incident angle of electron-dependent reflected angle of hole in the different directions of junction. The black (red dashed) line denotes the electron from D (D′) valley while the hole back to D′ (D) valley. Here $\varepsilon = 0.6\Delta_0$ and $E_F = \Delta_0$.

Generally, in a pristine graphene-based superconducting junction, the ARR (SAR) only appears in the regime of the intraband (interband) conversion of electron–hole. But, in a strain-modulated graphene-based superconducting junction, the ARR (SAR) can appear in the regime of the interband (intraband) conversion of electron–hole. The strain-induced anisotropic band structure of graphene, which breaks up the original relation between direction of velocity of particle and direction of the corresponding wavevector, leads to these two anomalous phenomena. In fact, the value of energy-gap function Δ_0 does not affect these two anomalous phenomena, i.e., interband-induced ARR and intraband-induced SAR. On the contrary, these two anomalous phenomena are affected by the tensile strain deeply. In Figs. 4(a) and 4(b), the numerical calculations show that the interband-induced ARR and the

intraband-induced SAR are not nearly modulated by energy-gap function Δ_0. But, in Figs. 4(c) and 4(d), it is easy to find that the larger ζ is, the more obvious these two anomalous phenomena are.

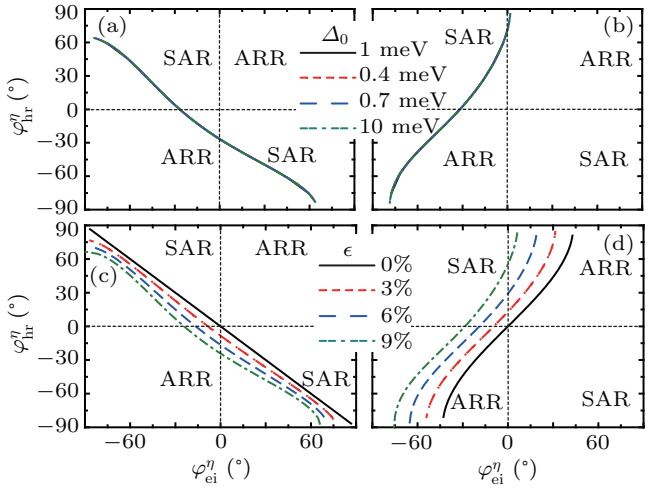


Fig. 4. The incident angle of electron-dependent reflected angle of hole in the different values of Δ_0 for $\varepsilon = 0.6\Delta_0$, $\zeta = 10\%$, $\theta = \pi/4$, and (a) $E_{\rm F} = 0$ or (b) $E_{\rm F} = \Delta_0$. The incident angle of electron-dependent reflected angle of hole in the different values of ζ for $\varepsilon = 0.6\Delta_0$, $\Delta_0 = 10$ meV, $\theta = \pi/4$, and (c) $E_{\rm F} = 0$ or (d) $E_{\rm F} = \Delta_0$. Here the electron comes from D valley while the hole goes back to D′ valley.

3.2. Perfect Andreev reflection

When the incident energy ε is smaller than energy-gap function Δ_0, it is easy to obtain $R^{\eta} + R^{\eta}_{\rm a} = 1$. Under certain conditions, the Andreev reflected probability $R^{\eta}_{\rm a}$ is always equal to 1, i.e., perfect Andreev reflection. In the coordinate x'–y' system, by using the Heisenberg's equation of motion, the velocity operator of electron along the x' direction is $\hat{u}_{x'\rm e} = \frac{1}{{\rm i}\hbar}[x', \mathcal{H}_{\eta} - E_{\rm F}\sigma_0] = \eta S_x$. The time evolution of $\hat{u}_{x'\rm e}$ is $\dot{\hat{u}}_{x'\rm e} = \frac{1}{{\rm i}\hbar}[\hat{u}_{{\rm e}x'}, \mathcal{H}_{\eta} - E_{\rm F}\sigma_0] = 2v_x v_y \sigma_z k_{y'}$. It is obvious that the velocity along the x' direction is conserved and the perfect Andreev reflection happens when $k_{y'} = 0$. In our model, the valley-dependent incident angle of perfect Andreev reflection is given by

$$\varphi^{\eta}_{\rm ei} = \arctan \frac{-\eta m v_{\rm t} + (v_y^2 - v_x^2)\cos\theta}{\eta m v_{\rm t}\cos\theta + m^2} \sin\theta, \tag{9}$$

where $m = \sqrt{v_x^2\cos^2\theta + v_y^2\sin^2\theta}$. We can obtain $\varphi^{\eta}_{\rm ei} = 0$ for $\theta = 0$, $\varphi^{+(-)}_{\rm ei} = -13.9°(-9.8°)$ for $\theta = \pi/4$, $\varphi^{+(-)}_{\rm ei} = -14.4°(-8.5°)$ for $\theta = \pi/3$, and $\varphi^{+(-)}_{\rm ei} = -4.3°(4.3°)$ for $\theta = \pi/2$.

In Fig. 5, incident angle-dependent R_{η} and $R^{\rm a}_{\eta}$ are plotted in $E_{\rm F} = 0$ and $\theta = 0$, $\pi/4$, $\pi/3$, and $\pi/2$. The incident angles of perfect Andreev reflection by numerical calculations is equal to the ones by solving Eq. (9). In Fig. 6 with $E_{\rm F} = \Delta_0$, the incident angles of perfect Andreev reflection are not changed, which means the perfect Andreev reflection is independent on Fermi energy. In Fig. 7, we give incident angles of perfect Andreev reflection in different directions of junction, where the incident angles is dependent on the conversion order of valley due to the strain-induced anisotropic band structure of graphene.

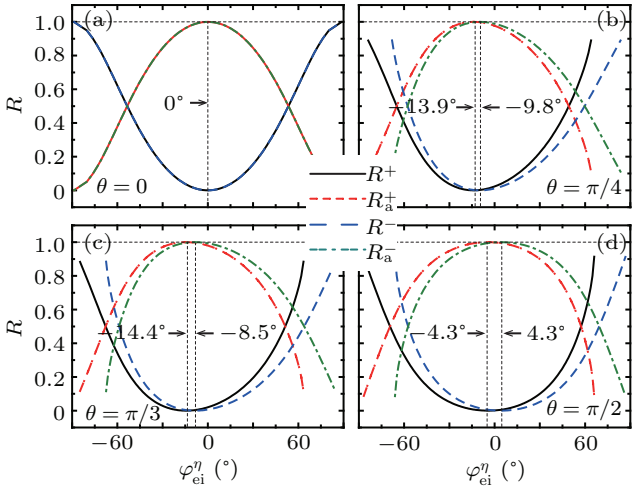


Fig. 5. (a)–(d) The reflected probabilities of electron and hole (R_{η} and $R^{\rm a}_{\eta}$) vs. the incident angle in different directions of junction. Here $\varepsilon = 0.6\Delta_0$, $U_0 = 15\Delta_0$, and $E_{\rm F} = 0$.

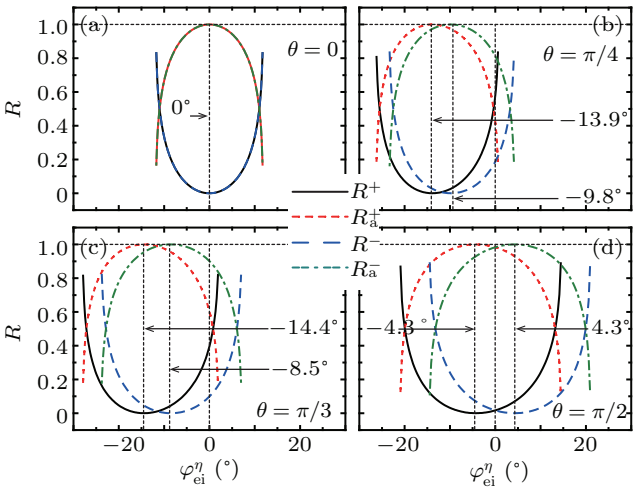


Fig. 6. (a)–(d) The reflected probabilities of electron and hole (R_{η} and $R^{\rm a}_{\eta}$) vs. the incident angle in different directions of junction. Here $\varepsilon = 0.6\Delta_0$, $U_0 = 15\Delta_0$, and $E_{\rm F} = \Delta_0$.

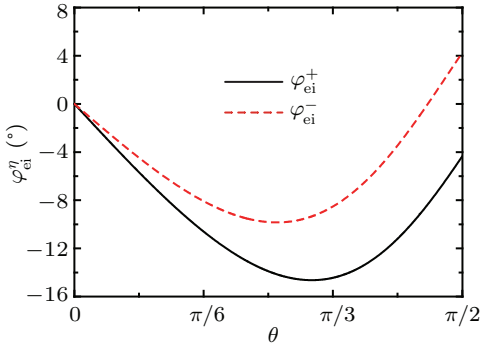


Fig. 7. Valley-dependent incident angle of perfect Andreev reflection $\varphi^{\eta}_{\rm ei}$ vs. the direction of junction θ for perfect Andreev reflection.

4. Conclusion

In conclusion, we discuss the Andreev reflection across a uniaxial strained graphene-based superconducting junction.

The band structure of graphene becomes anisotropic by applying a uniaxial strain, which induces three interesting phenomena: The Andreev retroreflection happens in the case of interband conversion of electron–hole, the intraband conversion of electron–hole results in the specular Andreev reflection, and the perfect Andreev reflection happens at a nonzero incident angle of electron. Our work provides an alternative and flexible method to tune Andreev reflection.

Acknowledgements

Project supported by the National Natural Science Foundation of China (Grant Nos. 12104232, 11805103, and 11804167), the Natural Science Foundation of Jiangsu Province, China (Grant Nos. BK20190137 and BK20180739), the Innovation Research Project of Jiangsu Province, China (Grant No. CZ0070619002), and NJUPT-SF (Grant No. NY218128).

References

[1] Novoselov K S, Geim A K, Morozov S V, Jiang D, Zhang Y, Dubonos S V, Grigorieva I V and Firsov A A 2004 *Science* **306** 666
[2] Zhang Y, Tan Y W, Stormer H L and Kim P 2005 *Nature* **438** 201
[3] Katsnelson M I, Novoselov K S and Geim A K 2006 *Nat. Phys.* **2** 620
[4] Beenakker C W J 2006 *Phys. Rev. Lett.* **97** 067007
[5] Kane C L and Mele E J 2005 *Phys. Rev. Lett.* **95** 146802
[6] Qiao Z, Tse W K, Jiang H, Yao Y and Niu Q 2011 *Phys. Rev. Lett.* **107** 256801
[7] Zhai X and Jin G 2014 *Phys. Rev. B* **89** 235416
[8] Wang W, Lü X and Xie H 2021 *Chin. Phys. B* **30** 066701
[9] Bistritzer R and MacDonald A H 2011 *Proc. Natl. Acad. Sci. USA* **108** 12233
[10] Cao Y, Fatemi V, Fang S, Watanabe K, Taniguchi T, Kaxiras E and Jarillo-Herrero P 2018 *Nature* **556** 43
[11] Tarnopolsky G, Kruchkov A J and Vishwanath A 2019 *Phys. Rev. Lett.* **122** 106405
[12] Yankowitz M, Chen S, Polshyn H, Zhang Y, Watanabe K, Taniguchi T, Graf D, Young A F and Dean C R 2019 *Science* **363** 1059
[13] de Abajo F J G 2013 *Science* **339** 917
[14] Koppens F, Mueller T, Avouris P, Ferrari A, Vitiello M and Polini M 2014 *Nat. Nanotechnol.* **9** 780
[15] Young A F and Kim P 2011 *Annual Review of Condensed Matter Physics* **2** 101
[16] Goerbig M O, Fuchs J N, Montambaux G and Piéchon F 2008 *Phys. Rev. B* **78** 045415
[17] Goerbig M O 2011 *Rev. Mod. Phys.* **83** 1193
[18] Andreev A F 1964 *Sov. Phys. JETP* **19** 1228
[19] Ludwig T 2007 *Phys. Rev. B* **75** 195322
[20] Zhang Q, Fu D, Wang B, Zhang R and Xing D Y 2008 *Phys. Rev. Lett.* **101** 047005
[21] Cheng S G, Xing Y, Wang J and Sun Q F 2009 *Phys. Rev. Lett.* **103** 167003
[22] Rainis D, Taddei F, Dolcini F, Polini M and Fazio R 2009 *Phys. Rev. B* **79** 115131
[23] Cheng S G, Zhang H and Sun Q F 2011 *Phys. Rev. B* **83** 235403
[24] Schelter J, Trauzettel B and Recher P 2012 *Phys. Rev. Lett.* **108** 106603
[25] Zhai X and Jin G 2014 *Phys. Rev. B* **89** 085430
[26] Linder J and Yokoyama T 2014 *Phys. Rev. B* **89** 020504
[27] Majidi L, Rostami H and Asgari R 2014 *Phys. Rev. B* **89** 045413
[28] Efetov D K, Wang L, Handschin C, Efetov K B, Shuang J, Cava R, Taniguchi T, Watanabe K, Hone J, Dean C R and Kim P 2015 *Nat. Phys.* **12** 328
[29] Sahu M R, Raychaudhuri P and Das A 2016 *Phys. Rev. B* **94** 235451
[30] Linder J and Yokoyama T 2017 *Phys. Rev. B* **95** 144515
[31] Li C X, Wang S K and Wang J 2017 *Chin. Phys. B* **26** 027304
[32] Qi F, Cao J, Cao J and Zhang L 2018 *Chin. Phys. B* **27** 127401
[33] Soori A, Sahu M R, Das A and Mukerjee S 2018 *Phys. Rev. B* **98** 075301
[34] Pandey P, Kraft R, Krupke R, Beckmann D and Danneau R 2019 *Phys. Rev. B* **100** 165416
[35] Wang C, Zhang L, Zhang P, Song J and Li Y X 2020 *Phys. Rev. B* **101** 045407
[36] Lv B, Zhang C and Ma Z 2012 *Phys. Rev. Lett.* **108** 077002
[37] Zhou X 2020 *Phys. Rev. B* **102** 045132
[38] Cheng R and Zhou X 2020 *Europhys. Lett.* **130** 17004
[39] Xu Y and Zhou X 2021 *Results in Physics* **27** 104523
[40] Zhu C Y, Xu W H, Zhou Y L, Ba J Y, Deng M X, Duan H J and Wang R Q 2021 *Phys. Rev. B* **103** 075148
[41] Zhou X 2019 *Phys. Rev. B* **100** 195139
[42] Lee C, Wei X, Kysar J W and Hone J 2008 *Science* **321** 385
[43] Garza H H P, Kievit E W, Schneider G F and Staufer U 2014 *Nano Lett.* **14** 4107